Cooperative Effect of Electrospinning and Nanoclay on Formation of Polar Crystalline Phases in Poly(vinylidene fluoride)

Yi-Liao Liu,[†] Ying Li,[†] Jun-Ting Xu,*[,†,‡] and Zhi-Qiang Fan*[,†,‡]

MOE Key Laboratory of Macromolecular Synthesis and Functionalization, Department of Polymer Science & Engineering, Zhejiang University, Hangzhou 310027, China, and State Key Laboratory of Chemical Engineering, Department of Chemical and Biological Engineering, Zhejiang University, Hangzhou 310027, China

ABSTRACT Poly(vinylidene difluoride)/organically modified montmorillonite (PVDF/OMMT) composite nanofibers were prepared by electrospinning the solution of PVDF/OMMT precursor in DMF. Wide-angle X-ray diffraction (WAXD) and transmission electron microscopy (TEM) show that in the bulk of the PVDF/OMMT precursor OMMT platelets are homogeneously dispersed in PVDF and can be both intercalated and exfoliated. It is found that the diameter of the PVDF/OMMT composite nanofibers is smaller than that of the neat PVDF fibers because the lower viscosity of PVDF/OMMT solution, which is attributed to the possible adsorption of PVDF chains on OMMT layers and thus reduction in number of entanglement. The crystal structure of the composite nanofibers was investigated using WAXD and Fourier transform infrared (FT-IR) and compared with that of thin film samples. The results show that the nonpolar α phase is completely absent in the electrospun PVDF/OMMT composite nanofibers, whereas it is still present in the neat PVDF electrospun fibers and in the thin films of PVDF/OMMT nanocomposites. The cooperative effect between electrospinning and nanoclay on formation of polar β and γ crystalline phases in PVDF is discussed. The IR result reveals that electrospinning induces formation of long trans conformation, whereas OMMT platelets can retard relaxation of PVDF chains and stabilize such conformation due to the possible interaction between the PVDF chains and OMMT layers. This cooperative effect leads to extinction of nonpolar α phase and enhances the polar β and γ phases in the electrospun PVDF/OMMT composite nanofibers.

KEYWORDS: poly(vinylidene fluoride) • electrospinning • clay • crystallization

INTRODUCTION

Poly(vinylidene difluoride) (PVDF) is a semicrystalline thermoplastic polymer with good mechanical and electrical properties, which attracts much interest because of its potential applications as piezoelectric, pyroelectric and ferroelectric materials. PVDF is able to crystallize in five different forms, which involve three different chain conformations, namely, *TTTT* for β phase, *TGTG′* for α and δ phases, *TTTGTTTG′* for γ and ε phases (1−3). Although each PVDF polymer chain has an effective molecular dipole moment, only the β and γ phases have dipole moment in the crystalline state. In contrast, the PVDF chains in the α phase stack with their respective polarizations in alternating directions, resulting in a paraelectric behavior, therefore it is nonpolar. The all-trans β phase is the most polar with the polymer chains stacking with their respective polarizations aligned in the same direction. As a consequence, enhancement of the content of the polar phases and suppression of the nonpolar α phase in PVDF material is of great importance for its applications. The β phase can be formed by high-pressure quenching from a melt or by casting from a strongly polar solvent (4−7). This phase can also be transformed from α phase by uniaxial or biaxial drawing (7−9).

Besides, two other methods are frequently used to enhance the content of β phase in PVDF as well as for improvement of other properties such as mechanical properties. The first is addition of layered silicate (often referred as nanoclay) into PVDF (9−18). In PVDF/nanoclay system, the effect of organically modified silicates on the crystalline structure of PVDF matrix has been studied intensively. Priya and Jog first prepared PVDF/nanoclay composites by melt intercalation and found that addition of organically modified silicates into PVDF films resulted in the formation of the β form (10−12). Giannelis et al. investigated the impact of unmodified and organically modified nanoclay on the crystalline structure of PVDF. The result showed that pristine layered silicate did not significantly change the crystal structure (13). They suggested that similar crystal lattices between the organically modified nanoclay and the β form should be the crucial factor to stabilize the β form, and the flat surface of the nanoclay facilitated intimate interaction between the polymer and nanoclay (13). Ramasundaram et al. proposed an ion-dipole interaction model to illuminate the interaction between exfoliated clay nanolayers and PVDF in the melt state (18). The existence of such ion-dipole interaction between negatively charged clay and positive CH_2 dipoles of PVDF resulted in preferential formation of the β phase. Electrospinning is another simple technique to form the β phase of PVDF nanofiber (19−24). Electrospinning

* Corresponding author. E-mail: xujt@zju.edu.cn.
Received for review March 23, 2010 and accepted May 12, 2010
[†] MOE Key Laboratory of Macromolecular Synthesis and Functionalization, Zhejiang University.
[‡] State Key Laboratory of Chemical Engineering, Zhejiang University.
DOI: 10.1021/am1002525

process involves the uniaxial stretching of a viscous polymer solution or melt in an electric field due to electrostatic repulsions between surface charges along the jet. Electrospinning of PVDF promotes the *TTTT* conformation and induces the formation of the β phase, possibly due to the highly extensional flow of the polymer solution (22).

It should be noted that only addition of nanoclay in PVDF or simple electrospinning of PVDF solution usually leads to coexistence of the nonpolar α phase with polar β and γ phases and difficulty in obtaining pure polar phases. Recently, to improve the properties of the nanofibers, electrospinning of polymer solution containing spherical, cylindrical, or lamellar nanoparticles has been reported (25−60). Andrew et al. prepared PVDF electrospun fibers with dispersed ferrite and found that the amount of β and γ phases in the fibers increased with the nanoparticle loading (58). Huang et al. demonstrated that electrospinning of PVDF with carbon nanotubes could induce highly oriented β form crystallites (59). Cebe et al. reported that organically modified nanoclay can eliminate the nonpolar α phase in PVDF nanofibers more effectively than unmodified nanoclay (60). The synergistic effect between electrospinning and addition of carbon nanotube or nanoclay has been deduced from the enhancement of the polar phases. However, the direct experimental evidence about the mechanism of the synergistic effect are still lacking.

In the present work, the PVDF/organically modified montmorillonite (OMMT) composite nanofibers were prepared by electrospinning. The aim of this work is to obtain PVDF nanofibers with pure polar crystalline phases by utilizing both the interaction between PVDF and nanoclay and the extensional force in electrospinning process. Special attention was paid to uncover the mechanism for the cooperative effect between these two factors.

EXPERIMENTAL SECTION

Materials. PVDF (Solef 1015) used in this study was obtained from Solvay (Brussels, Belgium) in powdery form with a weight-average molecular weight (M_w) of 970 000 g/mol. The organically modified montmorillonite (OMMT) nanoclay, Nanomer 1.44P, and unmodified montmorillonite, Nanomer PGW, were purchased from Nonocor Inc. (USA). The OMMT was prepared by the supplier, by ion-exchanging Na^+ MMT with dimethyl, dehydrogenated tallow.

Sample Preparation. PVDF/OMMT nanocomposites were prepared by coprecipitation method with the nanoclay loading of 1.0−3.0 wt %. First, PVDF was dissolved in *N*,*N*-dimethyl formamide (DMF) at 50 °C with a concentration of 5 w/v %. On the other hand, the nanoclay was dispersed in DMF and the OMMT/DMF mixture was sonicated at 50 °C for 60 min. The final solution was created by adding OMMT/DMF mixture to the PVDF/DMF solution. After further stirring for 12 h, the resultant mixture with a desired ratio of nanoclay to PVDF was poured into a 1 L beaker containing 500 mL deionized water and yellow stringy precipitate formed immediately. The precipitate and liquid was filtered under a vacuum and dried in a vacuum oven for 2 days at 60 °C.

For electrospinning operation, the PVDF/OMMT nanocomposites with different OMMT contents (0, 1, 2, and 3 wt %) prepared above were redissolved in DMF with a fixed solid/solvent ratio of 20 w/v %. The mixtures were kept stirring for 12 h and sonicated at room temperature for 30 min until dissolution. The solutions were then placed in a plastic syringe with an iron needle of tip-diameter 200 μm. Electrospinning was conducted at 15 kV at the feed rate of 0.5 mL/h. The collector was a grounded plate covered by aluminum foil. The distance between the needle and the collection plate is 15 cm. A composite nanofiber nonwoven mat was collected on the aluminum foil. All the electrospun fiber mats were dried in vacuum at room temperature overnight before characterization. The nanofibers electrospun from the PVDF solution containing OMMT were named as PCN-*m*-*n*, where m represented the weight percentage of the solid (PVDF and OMMT) in the electrospun solution and n represented the weight percentage of nanoclay in the PVDF/OMMT nanocomposites.

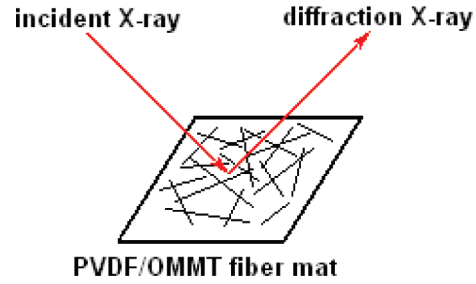

FIGURE 1. Schematic geometry of WAXD experiments for PVDF and PVDF/OMMT electrospun fibers.

For comparison, hot-press films were also prepared from the precipitated samples. A certain amount of the precipitated sample was placed between two stainless metal plates and pressed at 20 kpsi and at 200 °C for 5 min, then quenched into water. The obtained films were placed at 150 °C for 120 min, and cooled in air. The PVDF/OMMT nanocomposites films were named as PCN-*n*, where n represented the weight percentage of nanoclay in the nanocomposites.

The quenched films containing different loadings of nanoclays were also cut into strips of dumbbell shape (drawing region 20 × 6 mm). The samples were then drawn using a hot-tensile instrument at a rate of 0.27 mm/s with a real drawing ratio of approximately 6 at a drawing temperature of 130 °C. The drawn PVDF and PVDF/OMMT samples were used for Fourier transform Infrared (FT-IR) and optical microscope characterizations. For comparison, the drawn samples were also remelted at 180 °C for 10 min, and then cooled to 40 °C at a rate of 2 °C/min.

Characterization. Room temperature wide-angle X-ray diffraction (WAXD) experiments were performed on a Dmax/2550PC X-ray diffractometer with X-ray wavelength $\lambda = 0.1542$ nm, operated at 40 kV and 30 mA. The range of diffraction angle for investigation was $2\theta = 2-30°$ and the scanning step is 0.02°. For bulk PVDF/OMMT nanocomposites, hot-press films were used for WAXD experiments. For electrospun PVDF and PVDF/OMMT composite nanofibers, the collected fiber mats were used for WAXD characterization. The incident and diffraction X-ray beams are in the same plane vertical to the fiber mat, as shown in Figure 1.

Fourier transform Infrared (FT-IR) spectra were recorded on a Nicolet 6700 spectrometer equipped with an attenuated total reflectance (ATR) cell. The scanning range is from 4000 to 400 cm^{-1} with resolution of 4 cm^{-1}. For quantitative analysis, the FT-IR absorbance peaks were fitted with Laurentzian model after subtraction of baseline and the areas of the peaks were obtained.

The crystallinity of the electrospun nanofibers were determined by differential scanning calorimetry (DSC) method on a TA Q200 instrument. The crystallinity (X_c) is defined as $\Delta H_f/\Delta H_f^0$, where ΔH_f is the fusion enthalpy measured and ΔH_f^0 is the enthalpy for the 100% crystalline PVDF (104.6 J/g). Noting that the same values of ΔH_f^0 are used for the polar crystal phases and nonpolar crystal phase.

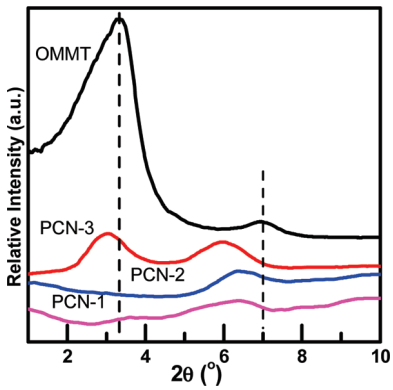

FIGURE 2. WAXD patterns of OMMT and PVDF/OMMT nanocomposites.

Transmission electron microscope (TEM) observations were carried out on a JEM-1230 TEM with an accelerating voltage of 80 kV. The PVDF/OMMT nanocomposite samples for TEM experiments were prepared using an ultramicrotome at room temperature.

The morphology of the electrospun fibers was examined with a JSM-55102 V scanning electron microscope (SEM) with an accelerating voltage of 25 kV. A thin layer of gold was sputtered on the sample surface before the examination.

Rheological characterizations of electrospinning solutions were performed on a stress controlled rheometer (AR-G2 rheometer, TA Instruments) using 40 mm diameter parallel plates at 25 °C. Tests were carried out in a gap of 0.5 mm. Dynamic strain sweeps at controlled frequency of 10 rad/s were conducted to confirm the linear and nonlinear regimes, and further rheological measurements in the linear regime were done at 5% strain. Small-amplitude oscillatory shear measurements were carried out within a frequency range of 0.01−600 rad/s. Storage modulus (G') and loss modulus (G'') were obtained by rheological test and the complex viscosity (η^*) was calculated as $\eta^* = [(G'/\omega)^2 + (G''/\omega)^2]^{1/2}$, where ω is the angular frequency.

The morphology of PVDF crystals was observed on Olympus BX-5 optical microscope equipped with a hot-stage and a digital camera. Transmitted light was employed and only one polarizer was used. Thin slices were cut from drawn sheets and melted at 180 °C on the hot-stage. After holding at 180 °C for 10 min, the samples were cooled to 40 °C at a rate of 2 °C/min, and then observations were performed at room temperature.

RESULTS AND DISCUSSION

Morphology PVDF/MMT Composites in Bulk. Before discussing the morphology and crystal structure of electrospun PVDF/MMT composite nanofibers, we first examine the dispersion of MMT in the bulk of PVDF/MMT nanocomposites. The PVDF/MMT nanocomposites were prepared by solution blending in DMF. After precipitation with nonsolvent and desiccation, the samples were used for characterization. Figure 2 shows the WAXD profiles of the pristine organically modified MMT (OMMT) and the PVDF/OMMT nanocomposites with various OMMT contents. A characteristic diffraction peak at 3.3° corresponding to the (001) plane of OMMT with a d-spacing of 2.64 nm is observed for the pristine OMMT. After blending with PVDF, the (001) diffraction peak of OMMT slightly shifts to a lower angle. This shows that a small portion of PVDF chains have intercalated into the galleries of OMMT, leading to increase of d-spacing. For PCN-3, the d-spacing is 2.92 nm (2θ = 3.0°), as compared with 2.64 nm for the pristine OMMT. For PCN-1 and PCN-2, the (001) diffraction peak of OMMT is much weak and the range of the peak is quite broad, indicating that a few of silicate layers are exfoliated in the PVDF matrix. Figure 3 shows the TEM images of the PVDF/OMMT nanocomposite with a OMMT loading of 2%. One can see from Figure 3 that the OMMT platelets are well-dispersed in PVDF matrix and large aggregates of OMMT are barely detected, though both intercalated and exfoliated nanoclay layers are observed. This observation is in accordance with WAXD results. Moreover, we observed a good orientation of the MMT platelets along the slicing direction produced during preparation of TEM samples. This shows that the compatibility between OMMT and PVDF is excellent, therefore the orientation of PVDF can drive the orientation of OMMT.

Morphology of the Electrospun Nanofibers. Figure 4 shows SEM images of neat PVDF and PVDF/OMMT nanofibers electrospun from their solutions in DMF. It is observed that the diameter of the neat PVDF nanofibers increases gradually with the concentration of the electrospun solution, which is about 300, 600, and 1000 nm when the concentration of the electrospun solution is 18, 20, and 22%, respectively (Figure 4a−c). It is also noticed that the diameter of the neat PVDF nanofibers becomes more and more uniform as the concentration of the electrospun solution increases. These findings agree with the reports in literature that increase in viscosity of the electrospun solution generally results in larger and more uniform diameter of the obtained nanofibers (19−21).

For comparison, the SEM images of PVDF/OMMT composite nanofibers electrospun from 20% solution in DMF with different amounts of OMMT were also shown in Figure 4 (Figure 4d−f). The difference in the fiber diameter is not evident for the three samples with different OMMT contents. However, when compared with the diameter of the neat PVDF nanofibers electrospun from the same concentration (20%), the diameters of the PVDF/OMMT composite nanofibers are obviously smaller. It is well-established that the diameter of the electrospun fibers is related to the zero-shear viscosity of the solution when the electrospinning conditions are identical (57, 61, 62). We measured the complex viscosity of PVDF-20 and PCN-20−2 solutions at the concentration of 20 wt/v% under dynamic shear. As shown in Figure 5, the complex viscosity of the PCN-2 solution is lower than that of the PVDF solution at lower frequency shear. Therefore we can deduce from Figure 5 that the PCN-20−2 solution has smaller zero-shear viscosity than the PVDF solution. In PEO/laponite electrospinning solution, it was believed that the laponite can adsorb PEO chains (63). Ramasundaram et al. also proposed that there exists an ion-dipole interaction between exfoliated clay nanolayers and PVDF chains (18), leading to conformations favorable to formation of polar β phase. It should be noted that the electrospinning solution is a concentrated solution and there are a large number of entanglements among the PVDF chains. Here, the rheological result strongly supports the

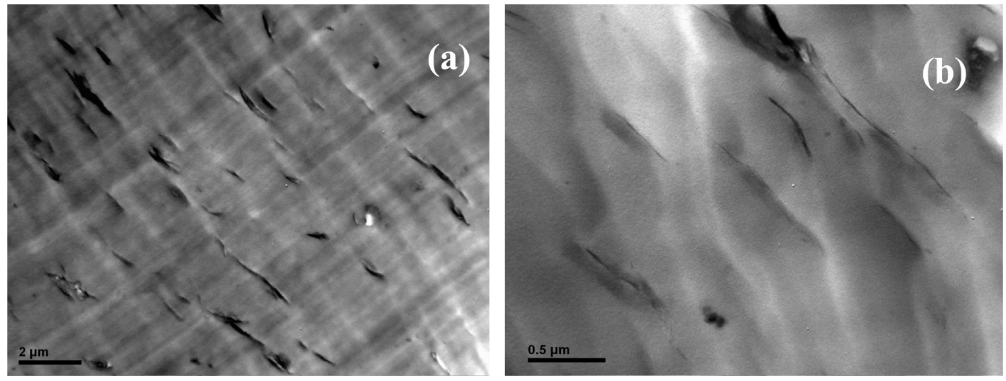

FIGURE 3. TEM images of PCN-2 nanocomposite.

presence of adsorption of PVDF chains on the surface of MMT, which may decrease the number of entanglement and thus lower the viscosity of the PVDF solution. Similar phenomenon has been reported in electrospinning of polyamide/OMMT solution (64).

The PVDF/OMMT composite nanofibers are also more irregular than the corresponding neat PVDF nanofibers, even a few beads or bead fibers are present in the mat as the amount of OMMT in the nanofiber increases. The change in local conductivity and viscosity is the main reason for the formation of irregular morphology, which may be related to the coexistence of different dispersion states of OMMT in PVDF including intercalated and exfoliated OMMT platelets. As the loading of OMMT increases, it is expected that OMMT tactoids will also be present.

Crystal Polymorphism in Electrospun Fibers. WAXD is a powerful tool to characterize crystal structure of polymer. The WAXD patterns of the electrospun fibers from neat PVDF and PVDF/OMMT solutions are shown in Figure 6. As can be seen from Figure 6, the neat PVDF fibers exhibit two diffraction peaks at $2\theta = 18.5$ and 20.0°, respectively. The peak at $2\theta = 18.5°$ corresponds to (020) reflection of the α phase, but it is severely overlapped with the amorphous halo. Both the (110) reflection of the α phase and the (200)/(110) reflections of the β phase produce diffraction peaks around $2\theta = 20.0°$ (65, 66). In the WAXD pattern of the PVDF/OMMT composite nanofibers, the peak at $2\theta = 18.5°$ becomes weak and the broad amorphous halo can be clearly seen. In addition, the peak at $2\theta = 20.0°$ shifts to $2\theta = 20.4°$. This result shows that the content of the polar β phase is possibly enhanced in the electrospun composite nanofibers (14). However, because the (110) reflection of the α phase and the (200)/(110) reflections of the β phase are severely overlapped, WAXD is not a good method for unambiguous indentification of the crystal structure of PVDF in the present work. As a result, FT-IR was used to further identify the crystal structure in the electrospun fibers.

FT-IR spectra of all the PVDF/OMMT composite nanofibers are shown in Figure 7a; for comparison, Figure 7b shows the FT-IR spectra of the hot-pressed PVDF/OMMT thin films. In the FT-IR spectra of PVDF, the bands at 764, 796, 976, 1150, 1214, and 1384 cm^{-1} correspond to the *TGTG′* conformer of α the crystal phase, and the bands at 842, 1234, and 1274 cm^{-1} are related to the trans sequences longer than *TT* (67). More specifically, the band at 1234 cm^{-1} is assigned to the *TTTG* conformation in the γ phase, which contains *TTTGTTTG′* conformation. The band at 1274 cm^{-1} is attributed to much longer trans sequences, which belongs to all trans conformation of β phase. The bands at 842 cm^{-1} is the absorbance of trans chains longer than *TT*, which is produced by both β and γ phases.

For the thin film samples, one can see that the relative intensities of the bands corresponding to the β and γ phases increase gradually as the content of OMMT increases, indicating that OMMT can induce the formation of β and γ phases to some extent. However, when comparing the FT-IR spectra of the PVDF/OMMT thin films and those of the neat PVDF nanofibers, we can see that the bands corresponding to the polar β and γ phases are much stronger in the neat PVDF nanofibers than those in the PVDF/OMMT thin films. This shows that electrospinning is more efficient in formation of the polar β and γ crystalline phases than addition of nanoclay. We notice that the nonpolar α phase is always present in the thin film samples, even for the sample containing 3% OMMT. There also exists α phase in the neat PVDF electrospun nanofibers, though the intensities of the bands due to the α phase are very weak. This shows simple electrospinning of PVDF solution or only addition of OMMT into the bulk of PVDF can not completely eliminate the nonpolar α phase. In contrast, the nonpolar α phase completely disappears in the composite nanofibers electrospun from PVDF/OMMT solutions, even for the sample containing only 1% OMMT.

To quantitatively characterize the content of polar crystalline phases in the composite nanofibers, the band at 1072 cm^{-1} is selected as a reference, which is regarded as only proportional to the sample thickness (68). All crystalline phases and amorphous phase contribute to this band. The area ratio of the FT-IR absorbance at 842 cm^{-1} (β- and γ-phases) with respect to the reference band ($A_{842\ cm^{-1}}/A_{1072\ cm^{-1}}$) is plotted as a function of OMMT content, as shown in Figure 8. It is found that the relative content of the polar crystal phases is enhanced in a loading of 1 wt % OMMT, but decreases with further increase in OMMT content. The data of absolute crystallinity determined by DSC are presented in Figure 8 as well. It shows that the crystallinities are 61.5, 60.7, 60.9, and 59.9%, respectively, for the

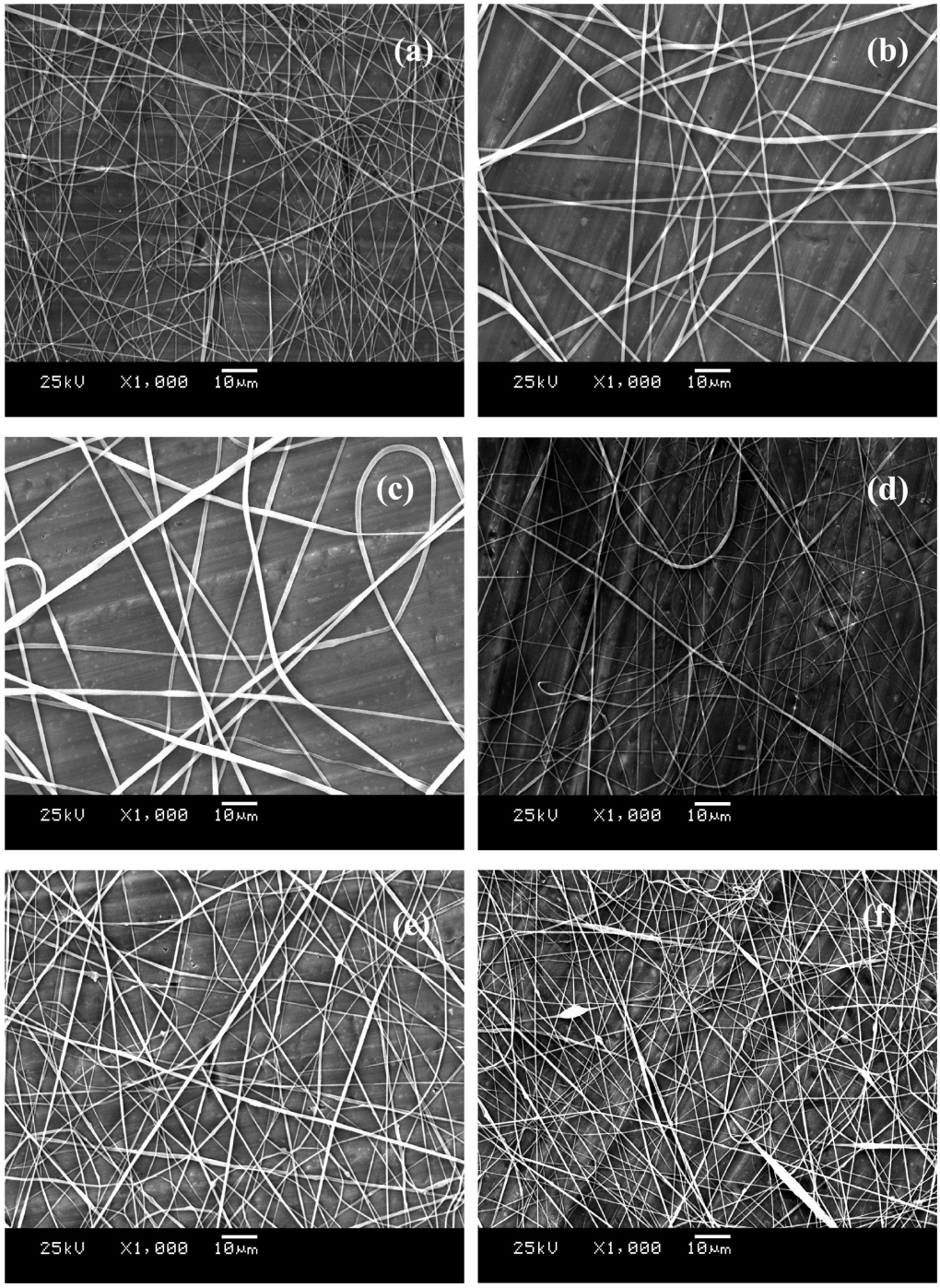

FIGURE 4. SEM images of electrospun composite nanofibers of PVDF/MMT with different nanoclay contents: (a) PVDF-18; (b) PVDF-20; (c) PVDF-22; (d) PCN-20-1; (e) PCN-20-2; (f) PCN-20-3.

electrospun nanofibers with OMMT loadings of 0, 1, 2, and 3%. This indicates that there is barely difference in the absolute crystallinity of the electrospun nanofibers with different OMMT loadings. As we can see, there exists discrepancy between the IR and DSC results for the content of the polar phases. Such a difference may originate from the different measurement mechanisms of IR and DSC. However, at least we can conclude that the content of the polar phases increases at low OMMT loading when combining FT-IT and DSC results.

Possible Mechanism for the Cooperative Effect. The FT-IR result reveals that electrospinning of the PVDF/OMMT solution can completely suppress the formation of nonpolar α crystalline phase, whereas electrospinning of PVDF solution or simple addition of OMMT into PVDF cannot eliminate the α crystalline phase. As a result, one question is raised: Is there any synergistic or cooperative effect between electrospinning and nanoclay on the formation of PVDF polar crystals? To answer this question, we designed the following experiment: Thin films of PVDF/OMMT nanocomposite first underwent tensile drawing. The stretched thin films were then melted at 180 °C for 10 min and cooled to room temperature for recrystallization. The contents of polar crystalline phases in the stretched thin

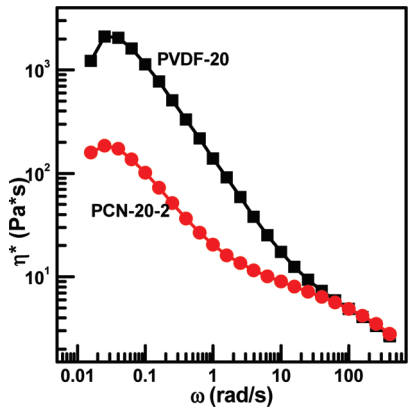

FIGURE 5. Plots of complex viscosity versus frequency for PVDF-20 and PCN-20-2 solutions.

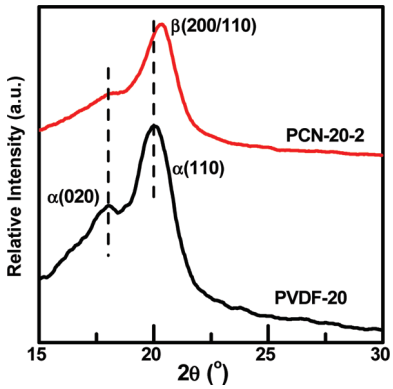

FIGURE 6. WAXD patterns of electron fibers of PDVF and PVDF/MMT composite.

films and melt-recrystallized thin films were investigated. For the convenience of morphological observation by optical microscopy, here we used thin film to substitute the nanofiber mat for study, because the extensional deformation of polymer chains occurs both in electrospinning and tensile drawing processes.

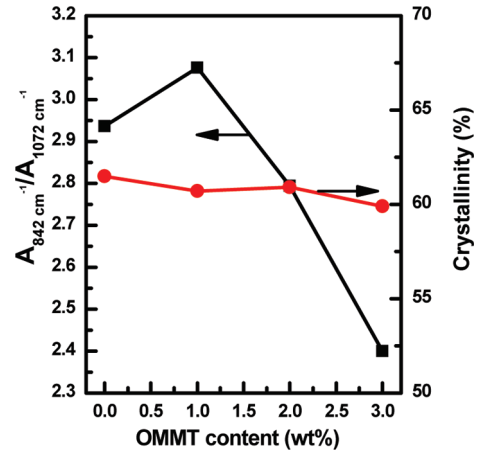

FIGURE 8. Plot of $A_{842\ cm^{-1}}/A_{1072\ cm^{-1}}$ versus OMMT content and crystallinity determined by DSC for the PVDF electrospun composite nanofibers.

Figure 9 shows the FT-IR spectra of the stretched PVDF and PCN-2 thin films before and after melting-recrystallization. One straight impression of the FT-IR spectra is that the bands corresponding to various crystalline phases become weak after melting-recrystallization due to decrease in crystallinity. However, one can see that the intensity of the band at 842 cm^{-1} due to polar β and γ decreases more severely than that of the band at 764 cm^{-1} due to nonpolar α crystalline phase for the neat PVDF thin film after melting-recrystallization. In contrast, the decrease in the intensity of the band at 842 cm^{-1} is not evident for the PVDF/OMMT

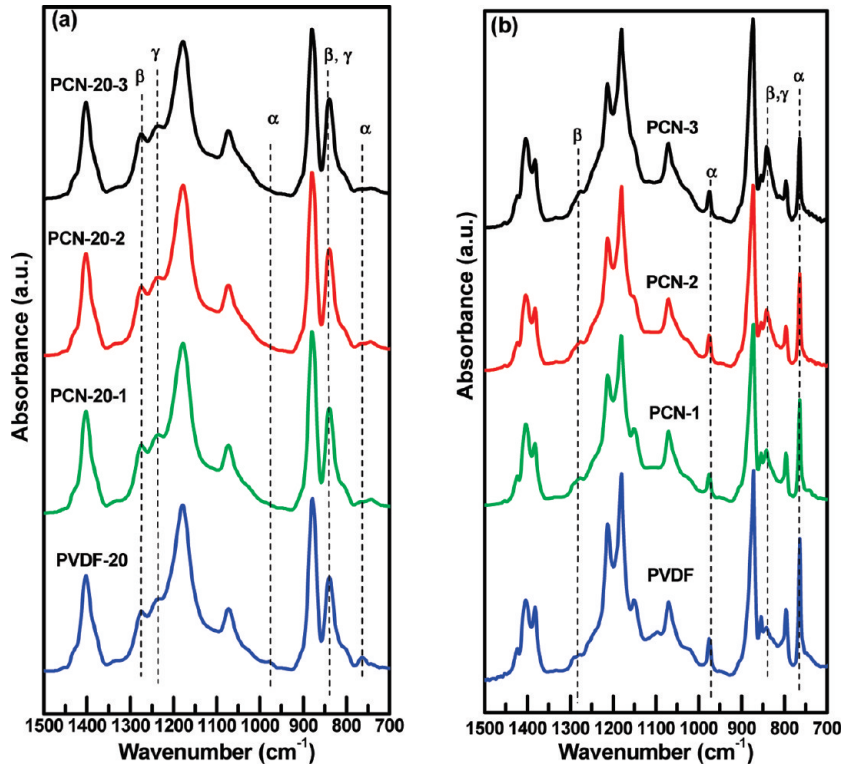

FIGURE 7. FT-IR spectra of PVDF and PVDF/OMMT samples. (a) electrospun fibers; (b) thin films.

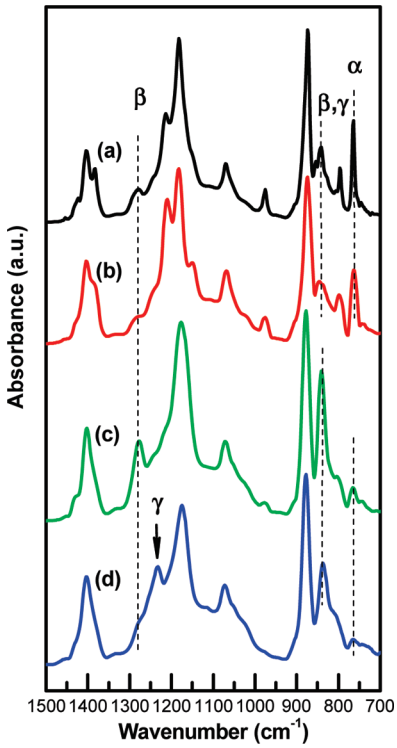

FIGURE 9. FT-IR spectra of PVDF and PVDF/OMMT thin films. (a) PVDF thin film after stretching for 600%; (b) melting-recrystallized PVDF thin film in a; (c) PVDF/OMMT thin film after stretching for 600%; (d) melting-recrystallized PVDF/OMMT thin film in c.

(PCN-2) thin film after melting-recrystallization. A parameter R is used to describe the retention ratio of the polar phases after melting-recrystallization for the stretched thin films, which is defined as:

$$R = \frac{(A_{842\text{cm}^{-1}}/A_{1072\text{cm}^{-1}})_m}{(A_{842\text{cm}^{-1}}/A_{1072\text{cm}^{-1}})_s} \quad (1)$$

Where $A_{842\ \text{cm}^{-1}}$ and $A_{1072\ \text{cm}^{-1}}$ are the areas of the bands at 842 and 1072 cm^{-1}, respectively. $(A_{842\ \text{cm}^{-1}}/A_{1072\ \text{cm}^{-1}})_s$ and $(A_{842\ \text{cm}^{-1}}/A_{1072\ \text{cm}^{-1}})_m$ represent the relative content of the polar phases in the stretched thin films and in the melting-recrystallized thin films, respectively.

The retention ratios of the polar phases after melting-recrystallization for different samples are shown in Figure 10. It is found that the retention ratio of the polar phases increases with the content of OMMT. The data in Figure 10 clearly show that the OMMT can stabilize the trans conformation in the polar crystalline phases. The more OMMT added, the stronger the stabilization effect. This is the first solid evidence for the stabilization effect of nanoclay on the conformation of PVDF, though such an effect has been inferred from the melting temperature after annealing by Priya (14). We also notice that in FT-IR spectra of the stretched PCN-2 thin film (Figure 9c,d), the band at 1234 cm^{-1} corresponding to γ crystalline phase becomes stronger after melting-recrystallization, whereas the band at 1274 cm^{-1} produced by the β phase becomes weaker. This indicates that most of the β crystals are converted into γ

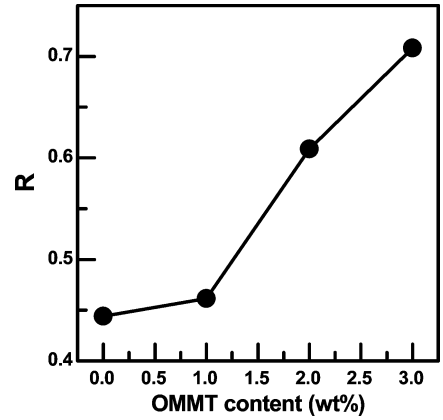

FIGURE 10. Retention ratio of the polar β and γ crystal phases after melting-recrystallization of the stretched PVDF and PVDF/OMMT thin films.

crystals after melting-recrystallization when OMMT is present. Considering the different conformations of PVDF in the β and γ phases, we infer that some of the trans conformers in the long *TTTT*... conformation sequences are transformed into isolated *G* or *G*′ conformers after melting-recrystallization, leading to formation of *TTTGTTTG*′ conformation in the γ crystalline phase.

Optical microscopy observation also confirms the stabilization effect of OMMT. Figure 11 shows that optical micrographs of the stretched PVDF and PCN-2 thin films before and after melting-recrystallization. The fiber-like crystals observed are β crystals (69). Crystals with good orientation are observed for both stretched thin films, but the crystal size in the PCN-2 thin film is smaller than that in the neat PVDF thin film due to the nucleation of the OMMT. After melting-recrystallization, the neat PVDF thin film becomes featureless. This is possibly due to the smaller size of the PVDF crystals. The neat PVDF sample also undergoes a dissolution−precipitation process as the PVDF/OMMT nanocomposites. Such a process has a purification effect on PVDF, resulting in difficulty in heterogeneous nucleation during crystallization, and thus spontaneous homogeneous nucelation is predominant and crystals of smaller size are formed. Anyway, no apparent orientation is observed for the stretched PVDF thin film after melting-recrystallization. In contrast, the orientation of the crystals in the PCN-2 thin film is retained to some extent, as indicated by the arrows in Figure 11d.

Combining above results obtained by various methods, we can give an overall picture about electrospinning of PVDF/OMMT (Figure 12). During electrospinning, the extensional flow of the polymer solution under electric field leads to orientation of polymer chains and this is the major factor that leads to formation of long trans conformation (as shown in Figure 7) (22). However, when OMMT is absent, relaxation can occur to the PVDF chains and the long trans conformers may be changed before crystallization. In contrast, when OMMT is added into the PVDF, relaxation of polymer chains is retarded and the long trans conformation is stabilized, as revealed by the melting-recrystallization experiment of the stretched PVDF/OMMT thin films. Even if relaxation of PVDF chains still occur, only some isolated *T* conformers are

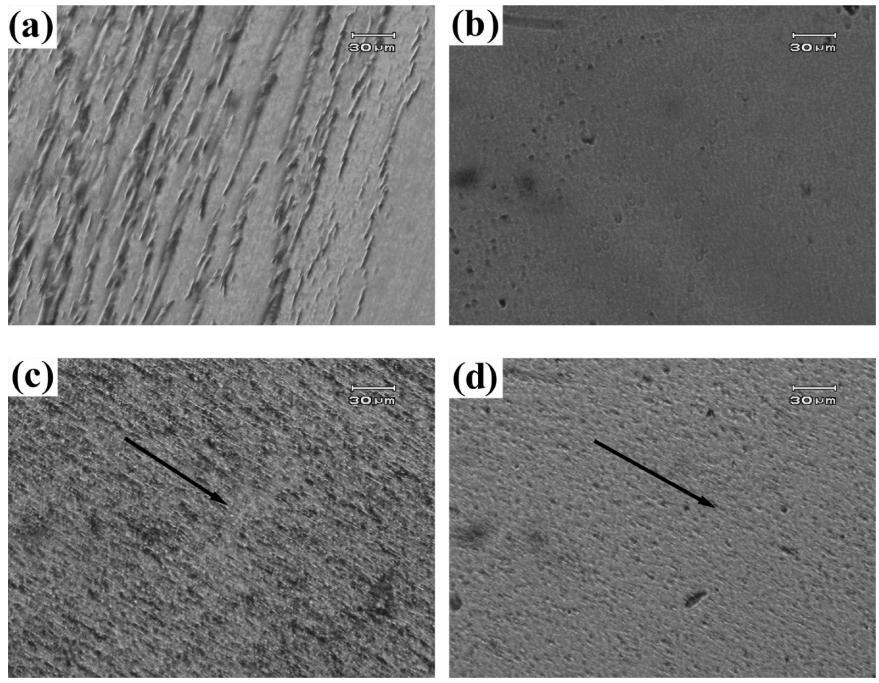

FIGURE 11. Optical micrographs of PVDF and PVDF/OMMT thin films. (a) PVDF thin film after stretching for 600%; (b) melting-recrystallized PVDF thin film in a; (c) PVDF/OMMT thin film after stretching for 600%; (d) melting-recrystallized PVDF/OMMT thin film in c.

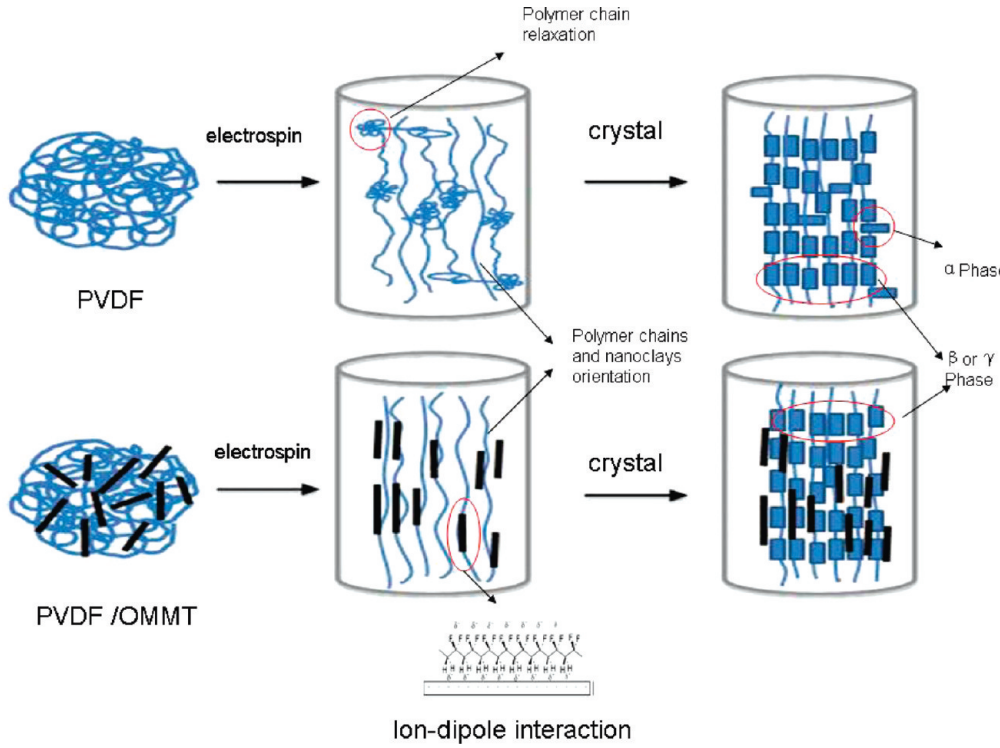

FIGURE 12. Schematic showing the proposed mechanism about electrospinning PVDF/OMMT composite fibers.

transformed into *G* or *G*′ conformers. The stabilization effect of nanoclay on long trans conformation shows that there exists an interaction between the PVDF chains and OMMT. The presence of such an interaction is supported by the lower zero-shear viscosity of the PVDF/OMMT electrospinning solution. The interaction between PVDF chains and OMMT nanoclay layers may decreases the number of entanglement, leading to viscosity. The stabilized long trans conformation is favorable to formation of polar β and γ phases upon crystallization. In a word, extensional flow caused by electrospinning and OMMT plays different but cooperative roles in formation of polar β and γ phases. This cooperative effect leads to complete elimination of nonpolar α phase and high content of polar β and γ phases in the electrospun PVDF/OMMT composite nanofibers.

One remaining question is the origin of the interaction between PVDF and OMMT. It can be either from PVDF/organic modifier interaction or from PVDF/MMT platelet

interaction. Therefore, unmodified MMT (PGW) was blended with PVDF and the corresponding composite nanofibers were prepared by electrospinning. We find that in the bulk of PVDF/unmodified MMT the dispersion of the MMT platelets is not so good as that of the organically modified MMT (see Figure S1 in the Supporting Information). However, the unmodified MMT can reduce the relative content of the nonpolar α phase and enhance the relative content of the polar phases in both thin film samples and in composite nanofibers (see Figure S2 in the Supporting Information). Compared with PVDF/OMMT composite nanofibers, the relative content of the nonpolar α phase is slightly higher in the PVDF/unmodified MMT composite nanofibers. As a result, the unmodified MMT can also reduce the nonpolar α phase as the organically modified MMT, but less efficiently than the organically modified MMT, possibly due to the worse dispersion of the unmodified MMT in PVDF. This shows that the interaction between PVDF and OMMT originates from PVDF/MMT platelets interacton, instead of from PVDF/ogranic modifier interaction. For the organically modified MMT, even though parts of the surface are covered by organic modifier, more surface will be exposed for interaction between PVDF and the MMT platelets after exfoliation. Such an interaction may be based on ion−dipole interaction, as proposed by Ramasundaram et al. (18).

CONCLUSION

PVDF/OMMT nanocomposites were successfully prepared by solution blending. The OMMT platelets are either exfoliated or intercalated and are homogeneously dispersed in PVDF. PVDF/OMMT composite nanofibers were prepared by electrospinning solution of PVDF/OMMT in DMF. The lower viscosity of PVDF/OMMT solution than the neat PVDF solution leads to smaller diameters of the composite nanofibers. FT-IR result reveals that nonpolar α phase completely disappears in the electrospun PVDF/OMMT composite nanofibers, whereas α phase can still be observed in PVDF electrospun fibers and in the bulk of PVDF/OMMT nanocomposites. Both electrospinning and addition of OMMT can enhance the content of polar β and γ phases. Melting-recrystallization of the stretched PVDF/OMMT thin films shows that OMMT can stabilize the long trans conformation. The cooperative effect between electrospinning and OMMT leads to complete elimination of nonpolar α phase and high content of polar β and γ phases in the electrospun PVDF/OMMT composite nanofibers.

Acknowledgment. This work was supported by National Basic Research Program of China (2005CB623804) and State Key Laboratory of Chemical Engineering (KL-ChE-10D04).

Supporting Information Available: TEM image of PVDF/unmodified MMT nanocomposite; WAXD profiles of thin films of the neat PVDF, PVDF/OMMT, and PVDF/unmodified MMT nanocomposites; FT-IR spectra of PVDF and PVDF/OMMT and PVDF/unmodified MMT (PGW-20-2) electrospun nanofibers (PDF). This material is available free of charge via the Internet at http://pubs.acs.org.

REFERENCES AND NOTES

(1) Lovinger, A. J. *Science* **1983**, *220*, 1115–1121.
(2) Guerra, G.; Karasz, F. E.; Macknight, W. J. *Macromolecules* **1986**, *19*, 1935–1938.
(3) Bharti, V.; Nath, R. *J. Phys. D: Appl. Phys.* **2001**, *34*, 667–672.
(4) Nalwa, H. S., *Ferroelectric Polymer: Chemistry, Physics and Applications*; Marcel Dekker: New York, 1995; pp 63−181.
(5) Ma, W. Z.; Zhang, J.; Chen, S. J.; Wang, X. L. *J. Macromol. Sci., Part B: Phys.* **2008**, *47*, 434–449.
(6) Ma, W. Z.; Zhang, J.; Wang, X. L. *J. Mater. Sci.* **2008**, *43*, 398–401.
(7) Gregorio, R. *J. Appl. Polym. Sci.* **2006**, *100*, 3272–3279.
(8) Lando, J. B.; Olf, H. G.; Peterlin, A. *J. Polym. Sci., Part A: Polym. Chem.* **1966**, *4*, 941–951.
(9) Pramoda, K. P.; Mohamed, A.; Phang, I. Y.; Liu, T. X. *Polym. Int.* **2005**, *54*, 226–232.
(10) Priya, L.; Jog, J. P. *J. Appl. Polym. Sci.* **2003**, *89*, 2036–2040.
(11) Priya, L.; Jog, J. P. *J. Polym. Sci., Part B: Polym. Phys.* **2002**, *40*, 1682–1689.
(12) Priya, L.; Jog, J. P. *J. Polym. Sci., Part B: Polym. Phys.* **2003**, *41*, 31–38.
(13) Shah, D.; Maiti, P.; Gunn, E.; Schmidt, D. F.; Jiang, D. D.; Batt, C. A.; Giannelis, E. R. *Adv. Mater.* **2004**, *16*, 1173–1177.
(14) Dillon, D. R.; Tenneti, K. K.; Li, C. Y.; Ko, F. K.; Sics, I.; Hsiao, B. S. *Polymer* **2006**, *47*, 1678–1688.
(15) Buckley, J.; Cebe, P.; Cherdack, D.; Crawford, J.; Ince, B. S.; Jenkins, M.; Pan, J. J.; Reveley, M.; Washington, N.; Wolchover, N. *Polymer* **2006**, *47*, 2411–2422.
(16) Song, Y. M.; Zhao, Z. D.; Yu, W. X.; Li, B.; Chen, X. F. *Sci. Chin. Ser. B-Chem.* **2007**, *50*, 790–796.
(17) Patro, T. U.; Mhalgi, M. V.; Khakhar, D. V.; Misra, A. *Polymer* **2008**, *49*, 3486–3499.
(18) Ramasundaram, S.; Yoon, S.; Kim, K. J.; Park, C. *J. Polym. Sci., Part B: Polym. Phys.* **2008**, *46*, 2173–2187.
(19) Nasir, M.; Matsumoto, H.; Danno, T.; Minagawa, M.; Irisawa, T.; Shioya, M.; Tanioka, A. *J. Polym. Sci., Part B: Polym. Phys.* **2006**, *44*, 779–786.
(20) Yee, W. A.; Kotaki, M.; Liu, Y.; Lu, X. H. *Polymer* **2007**, *48*, 512–521.
(21) Zheng, R.; He, A.; Li, J.; Han, C. C. *Macromol. Rapid Commun.* **2007**, *28*, 2159–2162.
(22) Andrew, J. S.; Clarke, D. R. *Langmuir* **2008**, *24*, 670–672.
(23) Huang, F. L.; Wei, Q. F.; Wang, J. X.; Cai, Y. B.; Huang, Y. B. *e-Polym.* **2008**, No.152.
(24) Yee, W. A.; Nguyen, A. C.; Lee, P. S.; Kotaki, M.; Liu, Y.; Tan, B. T.; Mhaisalkar, S.; Lu, X. H. *Polymer* **2008**, *49*, 4196–4203.
(25) Dror, Y.; Salalha, W.; Khalfin, R. L.; Cohen, Y.; Yarin, A. L.; Zussman, E. *Langmuir* **2003**, *19*, 7012–7020.
(26) Hou, H. Q.; Ge, J. J.; Zeng, J.; Li, Q.; Reneker, D. H.; Greiner, A.; Cheng, S. Z. D. *Chem. Mater.* **2005**, *17*, 967–973.
(27) Kim, G. M.; Michler, G. H.; Potschke, P. *Polymer* **2005**, *46*, 7346–7351.
(28) Sundaray, B.; Subramanian, V.; Natarajan, T. S.; Krishnamurthy, K. *Appl. Phys. Lett.* **2006**, *88*, No.143114.
(29) Seoul, C.; Kim, Y. T.; Baek, C. K. *J. Polym. Sci., Part B: Polym. Phys.* **2003**, *41*, 1572–1577.
(30) Wang, A.; Hsieh, A. J.; Rutledge, G. C. *Polymer* **2005**, *46*, 3407–3418.
(31) Kim, G. M.; Lach, R.; Michler, G. H.; Chang, Y. W. *Macromol. Rapid Commun.* **2005**, *26*, 728–733.
(32) Hong, J. H.; Jeong, E. H.; Lee, H. S.; Baik, D. H.; Seo, S. W.; Youk, J. H. *J. Polym. Sci., Part B: Polym. Phys.* **2005**, *43*, 3171–3177.
(33) Lee, Y. H.; Lee, J. H.; An, I. G.; Kim, C.; Lee, D. S.; Lee, Y. K.; Nam, J. D. *Biomaterials* **2005**, *26*, 3165–3172.
(34) Mei, F.; Zhong, J. S.; Yang, X. P.; Ouyang, X. Y.; Zhang, S.; Hu, X. Y.; Ma, Q.; Lu, J. G.; Ryu, S.; Deng, X. L. *Biomacromolecules* **2007**, *8*, 3729–3735.
(35) Fong, H.; Liu, W. D.; Wang, C. S.; Vaia, R. A. *Polymer* **2002**, *43*, 775–780.
(36) Mack, J. J.; Viculis, L. M.; Ali, A.; Luoh, R.; Yang, G. L.; Hahn, H. T.; Ko, F. K.; Kaner, R. B. *Adv. Mater.* **2005**, *17*, 77–80.
(37) Ji, Y.; Li, B. Q.; Ge, S. R.; Sokolov, J. C.; Rafailovich, M. H. *Langmuir* **2006**, *22*, 1321–1328.
(38) Li, L.; Bellan, L. M.; Craighead, H. G.; Frey, M. W. *Polymer* **2006**, *47*, 6208–6217.

(39) Kim, G. M.; Michler, G. H.; Ania, F.; Calleja, F. J. B. *Polymer* **2007**, *48*, 4814–4823.
(40) Jose, M. V.; Steinert, B. W.; Thomas, V.; Dean, D. R.; Abdalla, M. A.; Price, G.; Janowski, G. M. *Polymer* **2007**, *48*, 1096–1104.
(41) Marras, S. I.; Kladi, K. P.; Tsivintzelis, L.; Zuburtikudis, I.; Panayiotou, C. *Acta Biomater.* **2008**, *4*, 756–765.
(42) Chen, D.; Liu, T. X.; Zhou, X. P.; Tjiu, W. C.; Hou, H. Q. *J. Phys. Chem. B* **2009**, *113*, 9741–9748.
(43) Lee, H. W.; Karim, M. R.; Ji, H. M.; Choi, J. H.; Do Ghim, H.; Park, S. M.; Oh, W.; Yeum, J. H. *J. Appl. Polym. Sci.* **2009**, *113*, 1860–1867.
(44) Ji, H. M.; Lee, H. W.; Karim, M. R.; Cheong, I. W.; Bae, E. A.; Kim, T. H.; Islam, M. S.; Ji, B. C.; Yeum, J. H. *Colloid Polym. Sci.* **2009**, *287*, 751–758.
(45) Ji, J. Y.; Sui, G.; Yu, Y. H.; Liu, Y. X.; Lin, Y. H.; Du, Z. J.; Ryu, S.; Yang, X. P. *J. Phys. Chem. C* **2009**, *113*, 4779–4785.
(46) Kang, M. S.; Shinb, M. K.; Ismail, Y. A.; Shin, S. R.; Kim, S. I.; Kim, H.; Lee, H.; Kim, S. J. *Nanotechnology* **2009**, *20*, No.085701.
(47) Cai, Y. B.; Li, Q.; Wei, Q. F.; Wu, Y. B.; Song, L.; Hu, Y. *J. Mater. Sci.* **2008**, *43*, 6132–6138.
(48) Blond, D.; Walshe, W.; Young, K.; Blighe, F. M.; Khan, U.; Almecija, D.; Carpenter, L.; McCauley, J.; Blau, W. J.; Coleman, J. N. *Adv. Funct. Mater.* **2008**, *18*, 2618–2624.
(49) Naebe, M.; Lin, T.; Staiger, M. P.; Dai, L. M.; Wang, X. G. *Nanotechnology* **2008**, *19*, 8.
(50) Feng, W.; Wu, Z. G.; Li, Y.; Feng, Y. Y.; Yuan, X. Y. *Nanotechnology* **2008**, *19*, No.105707.
(51) Zhang, Q. H.; Chang, Z. J.; Zhu, M. F.; Mo, X. M.; Chen, D. J. *Nanotechnology* **2007**, *18*, No.115611.
(52) Zussman, E.; Yarin, A. L.; Bazilevsky, A. V.; Avrahami, R.; Feldman, M. *Adv. Mater.* **2006**, *18*, 348–353.
(53) Sen, R.; Zhao, B.; Perea, D.; Itkis, M. E.; Hu, H.; Love, J.; Bekyarova, E.; Haddon, R. C. *Nano Lett.* **2004**, *4*, 459–464.
(54) Ko, F.; Gogotsi, Y.; Ali, A.; Naguib, N.; Ye, H. H.; Yang, G. L.; Li, C.; Willis, P. *Adv. Mater.* **2003**, *15*, 1161–1165.
(55) Ye, H. H.; Lam, H.; Titchenal, N.; Gogotsi, Y.; Ko, F. *Appl. Phys. Lett.* **2004**, *85*, 1775–1777.
(56) Salalha, W.; Dror, Y.; Khalfin, R. L.; Cohen, Y.; Yarin, A. L.; Zussman, E. *Langmuir* **2004**, *20*, 9852–9855.
(57) Daga, V. K.; Helgeson, M. E.; Wagner, N. J. *J. Polym. Sci., Part B: Polym. Phys.* **2006**, *44*, 1608–1617.
(58) Andrew, J. S.; Clarke, D. R. *Langmuir* **2008**, *24*, 8435–8438.
(59) Huang, S.; Yee, W. A.; Tjiu, W. C.; Liu, Y.; Kotaki, M.; Boey, Y. C. F.; Ma, J.; Liu, T. X.; Lu, X. H. *Langmuir* **2008**, *24*, 13621–13626.
(60) Yu, L.; Cebe, P. *Polymer* **2009**, *50*, 2133–2141.
(61) Drew, C.; Wang, X. Y.; Samuelson, L. A.; Kumar, J. *J. Macromol. Sci. Part A-Pure Appl. Chem.* **2003**, *A40*, 1415–1422.
(62) McKee, M. G.; Wilkes, G. L.; Colby, R. H.; Long, T. E. *Macromolecules* **2004**, *37*, 1760–1767.
(63) Baghdadi, H. A.; Sardinha, H.; Bhatia, S. R. *J. Polym. Sci., Part B: Polym. Phys.* **2005**, *43*, 233–240.
(64) Li, Q.; Wei, Q. F.; Wu, N.; Cai, Y. B.; Gao, W. D. *J. Appl. Polym. Sci.* **2008**, *107*, 3535–3540.
(65) Bachmann, M. A.; Lando, J. B. *Macromolecules* **1981**, *14*, 40–46.
(66) Hasegawa, R.; Takahash, Y.; Tadokoro, H.; Chatani, Y. *Polym. J.* **1972**, *3*, 600–610.
(67) Kobayashi, M.; Tashiro, K.; Tadokoro, H. *Macromolecules* **1975**, *8*, 158–171.
(68) Benz, M.; Euler, W. B. *J. Appl. Polym. Sci.* **2003**, *89*, 1093–1100.
(69) Shah, D.; Maiti, P.; Jiang, D. D.; Batt, C. A.; Giannelis, E. P. *Adv. Mater.* **2005**, *17*, 525–528.

AM1002525